Rheol Acta (2009) 48:317–331
DOI 10.1007/s00397-008-0321-0

ORIGINAL CONTRIBUTION

A mesoscopic tube model of polymer/layered silicate nanocomposites

Hassan Eslami · Miroslav Grmela · Mosto Bousmina

Received: 8 April 2008 / Accepted: 16 September 2008 / Published online: 5 November 2008

Abstract Rheology of isothermal suspensions of completely exfoliated silicate lamellae in polymer melts is investigated. In order to express more faithfully the physics involved in low shear rates and low frequencies, we model the polymer molecules composing the melt as chains whose motion is confined to a tube formed by surrounding chains and lamellae. In the absence of lamellae, the model reduces to the mesoscopic model of reptating chains developed in Eslami and Grmela (Rheol Acta, 2008). If the chains are seen only as FENE-P dumbbells, the model reduces to the model developed in Eslami et al. (J Rheol 51:1189–1222, 2007). Responses to oscillatory, transient, and steady shear flows are calculated and compared with available experimental data. Particular attention is payed to the region of low shear rate and low frequency.

Keywords Tube model · Nanocomposite · Rheological model

H. Eslami · M. Grmela (✉)
Center for Applied Research on Polymers and Composites (CREPEC), Ecole Polytechnique de Montreal, C.P.6079 suc. Centre-ville, Montreal, H3C 3A7, Quebec, Canada
e-mail: miroslav.grmela@polymtl.ca

M. Bousmina
Canada Research Chair on Polymer Physics and Nanotechnology and Center for Applied Research on Polymers and Composites (CREPEC), Department of Chemical Engineering, Laval University, Ste-Foy, G1K 7P4, Quebec, Canada

M. Bousmina
Hassan II Academy of Sciences and Technology, Rabat, Morocco

Introduction

The physical system investigated in this paper is the same as in Eslami et al. (2007). It is an incompressible and isothermal suspension of homogeneously distributed and completely exfoliated clay lamellae in polymer melts. In the model formulated in Eslami et al. (2007) (hereafter called model I), the polymer macromolecules composing the melt are represented by FENE-P dumbbells. The model includes the lamella–lamella and lamella–polymer interactions, it is formulated on a mesoscopic level on which conformation tensors serve as microstructural state variables and in the modular framework of GENERIC. As for the results, predictions of nonlinear rheology are relatively easily calculated (the calculations consist of solving a system of ordinary differential equations) and show a good agreement with results of experimental observations except for the measurements revealing the long-range structures (i.e., low-deformation nonlinear rheology and low-frequency linear rheology). The objective of this paper is to extend model I to include the physics involved in the larger structures.

We make two modifications of model I. First, we replace the FENE-P dumbbells with reptating chains. The motion of one selected chain is constrained by a tube formed by surrounding chains and surrounding lamellae. On the mesoscopic level of description adopted in this paper, the reptating motion is expressed mathematically as a diffusion alongside the backbone of the chain and the lamellae participation in the reptation as a coupling of the diffusion to the conformation of the plates. Microscopic details about the influence of the lamellae on the motion of the chains is out of the reach of the mesoscopic description. The second

modification that we are introducing in model II is that the renormalization of the number densities of the polymer molecules and the lamellae are allowed to depend on the concentration of the lamellae. The renormalization is needed in model I, as well as in the model developed in this paper (hereafter called model II) in order to resolve in the mathematical formulation, which uses only one-chain and one-lamella characterizations, the disparity of sizes of lamellae and polymer molecules. As in (Eslami et al. 2007), model II is constructed in the framework of GENERIC. In the absence of lamellae, model I reduces to the FENE-P model and model II to the mesoscopic tube model developed in Eslami and Grmela (2008).

The paper is organized as follows. In the "Model formulation" section, we formulate the governing equations of the model. In the "Results and discussion" section, we present the results and compare them with results of experimental observations (in particular, the results collected in the low deformation nonlinear rheology and low-frequency linear rheology).

Model formulation

Classical hydrodynamics begins with a general framework for the time evolution equations whose solutions are guaranteed to agree with the observed conservation of the total mass, the total energy, and the total momentum. The framework (the local balance laws) is then filled with the particular physics of the particular fluid under consideration in the second step, called a specification of constitutive relations. The second step becomes very difficult for complex fluids (for example, for the suspensions discussed in this paper). In order to simplify it, we may suggest to begin by modifying the first step. This type of extension of the strategy of classical hydrodynamics, suitable in particular to complex fluids, is called GENERIC (Grmela and Ottinger 1997; Ottinger and Grmela 1997).

Instead of requiring just mass, energy, and momentum conservations, we require more. Solutions to the governing equations are required to be compatible with mechanics and with thermodynamics. The former requirement means that, in the absence of dissipation, the dynamics is Hamiltonian; the latter means that solutions of the governing equations approach (in the absence of external forces) equilibrium states at which the equilibrium thermodynamics is applicable. The framework for equations possessing the properties mentioned above is called GENERIC. Its main advantage is the wide range of applicability. The GENERIC framework is formulated for any set of state variables, while the framework of classical hydrodynamics is formulated only for the classical hydrodynamic fields. The complex fluids are complex because they have an internal structure that evolves in time on a scale comparable to the scale on which the classical hydrodynamic fields evolve. The internal structure has to be thus represented in the state variables and in the time evolution. Consequently, the framework of classical hydrodynamics (a set of local balance laws for the classical hydrodynamic fields) does not apply to complex fluids.

The GENERIC framework is recalled in the Appendix. The GENERIC constitutive relations representing the nano suspension are discussed in the next section.

GENERIC constitutive relations

Hereafter, we limit ourselves to isothermal fluids. In order to transform Eq. 18 into equations governing the time evolution of the nano suspension discussed in this paper, we have to express the particular physics of the suspension in the specification of x, L, Ξ, Φ, called GENERIC constitutive relations. We shall make the specifications, one after the other, below.

State variables

Beside being isothermal and incompressible, we consider the suspension under consideration in this paper to be spatially homogeneous. The state variables are thus independent of the position vector $\boldsymbol{r}$.

The polymer molecules composing the polymer melts are regarded as chains. States of the melt in tube theories (De Gennes 1971; Doi and Edwards 1986; Likhtman and McLeish 2002; McLeish 2002) are characterized by one chain configuration space distribution function $\psi(\boldsymbol{R}, s)$, where $\boldsymbol{R}$ is the vector tangent to the chain and $-1 \leq s \leq 1$ is the coordinate on the backbone of the chain. We follow (Eslami and Grmela 2008) and choose the conformation tensor $\boldsymbol{c}(s)$ to characterize states of chains. The conformation tensor is a symmetric positive definite three-by-three tensor. It has the physical interpretation of the deformation tensor. It can also be interpreted as a second moment of $\psi(\boldsymbol{R}, s)$. By choosing $\boldsymbol{c}$ instead of ψ, we gain the simplicity in solving the governing equations but we loose the richness of details of the physics that we can express. Results reported in Eslami and Grmela (2008) indicate that the details we lose are of lesser importance in the investigation of the rheological behavior of our interest.

Now, we have to decide what the variables that we shall use to describe states of the lamellae are. In this paper, we make the simplest choice. Let $\boldsymbol{n}$ be a unit

vector perpendicular to the lamella. The distribution of the lamellae for homogeneous distribution is described by the distribution function $\psi(\boldsymbol{n})$. Its second moment is a tensor denoted by the symbol $\boldsymbol{a}$ (i.e., $a_{\alpha\beta} = \int d\boldsymbol{n} n_\alpha n_\beta \psi(\boldsymbol{n})$). The constraint $|\boldsymbol{n}| = 1$ is expressed on the conformation tensor level as $tr\boldsymbol{a} = 1$. This means that the surface area of one lamella remains unchanged during the time evolution.

Altogether, the state variables considered in this paper are:

$$(\boldsymbol{u}(\boldsymbol{r}),\ \boldsymbol{c}(s),\ \ \boldsymbol{a})\,;\quad tr(\boldsymbol{a}) = 1, \tag{1}$$

where $\boldsymbol{u}(\boldsymbol{r})$ is the field of momentum. In the context of rheology, the momentum field is imposed from outside. In accordance with our assumption of spatial homogeneity, we shall consider below only $\boldsymbol{u}$ that depends linearly on $\boldsymbol{r}$.

Kinematics

We use the same kinematics for $\boldsymbol{c}(s)$ as in Eslami and Grmela (2008) and for $\boldsymbol{a}$ as in Eslami et al. (2007). We therefore write directly the nondissipative time evolution equations, i.e., the first term on the right-hand side of Eq. 18:

$$\frac{\partial u_\alpha}{\partial t} = -\partial_\beta \left(\frac{u_\alpha u_\beta}{\rho}\right) - \partial_\alpha p - \partial_\beta \sigma_{\alpha\beta} \tag{2}$$

$$\frac{\partial c_{\alpha\beta}}{dt} = -\frac{1}{2}\left(\boldsymbol{\Omega}\cdot\boldsymbol{c} - \boldsymbol{c}\cdot\boldsymbol{\Omega}\right)_{\alpha\beta} + \frac{1}{2}\left(\dot{\boldsymbol{\gamma}}\cdot\boldsymbol{c} + \boldsymbol{c}\cdot\dot{\boldsymbol{\gamma}}\right)_{\alpha\beta} \tag{3}$$

$$\frac{d\boldsymbol{a}}{dt} = -\frac{1}{2}\left(\boldsymbol{\Omega}\cdot\boldsymbol{a} - \boldsymbol{a}\cdot\boldsymbol{\Omega}\right) + \xi\left(-\frac{1}{2}\left(\dot{\boldsymbol{\gamma}}\cdot\boldsymbol{a} + \boldsymbol{a}\cdot\dot{\boldsymbol{\gamma}}\right) + tr(\boldsymbol{a}\,.\,\dot{\boldsymbol{\gamma}})\boldsymbol{a}\right) \tag{4}$$

and the expression for the extra stress tensor $\boldsymbol{\sigma}$ corresponding to them

$$\sigma_{\alpha\beta} = -2\int_{-1}^{1} ds\, c_{\alpha\varepsilon}\Phi_{c_{\varepsilon\beta}} + 2\,\xi\, a_{\alpha\varepsilon}\Phi_{a_{\varepsilon\beta}} - 2\,\xi\, a_{\alpha\beta}\, tr(\boldsymbol{a}\,.\,\Phi_{\boldsymbol{a}}) \tag{5}$$

By $\dot{\boldsymbol{\gamma}}_{\alpha\beta} = \frac{\partial\Phi_{u_\alpha}}{\partial r_\beta} + \frac{\partial\Phi_{u_\beta}}{\partial r_\alpha}$ and $\boldsymbol{\Omega}_{\alpha\beta} = \frac{\partial\Phi_{u_\alpha}}{\partial r_\beta} - \frac{\partial\Phi_{u_\beta}}{\partial r_\alpha}$, we denote the strain rate and the vorticity tensor, respectively; $\alpha, \beta = 1, 2, 3$. We use in Eq. 5 and in the rest of the paper the summation convention (i.e., summation over repeated indices). Note that Eq. 4 implies $dtr\boldsymbol{a}/dt = 0$.

The advection of $\boldsymbol{c}(s)$ and of $\boldsymbol{a}$ is different because of the following three differences in the tensors $\boldsymbol{c}(s)$ and $\boldsymbol{a}$: (1) the tensors $\boldsymbol{c}(s)$ are unconstrained and the tensor $\boldsymbol{a}$ is constrained by $tr\boldsymbol{a} = 1$; (2) $\boldsymbol{c}(s)$ are the second moments of the vector that itself is advected by the flow, while $\boldsymbol{a}$ is the second moment of the vector that is perpendicular to the plate that is advected by the flow; and (3) the advection of $\boldsymbol{c}$ is affine and the advection of $\boldsymbol{a}$, involving the parameter ξ, is nonaffine. The nonaffine modification of the advection makes the nondissipative time evolution non-Hamiltonian. It should be seen as an approximation of an active advection, introduced in Gu and Grmela (2008), that is Hamiltonian. The formula Eq. 5 arises as a consequence of the Hamiltonian structure. In the case of the nonaffine (i.e., non-Hamiltonian) advection, the formula Eq. 5 can be derived from thermodynamic considerations (Grmela 1985). In this paper, we consider ξ to be a phenomenological parameter. We note that it is the only phenomenological parameter entering the nondissipative time evolution. All the other parameters expressing the individual nature of the suspension will enter in the dissipative part.

Dissipation

From the general formulation (see Appendix), we know that the dissipation potential Ξ is a function of $\Phi_{\boldsymbol{c}(s)}$ and $\Phi_{\boldsymbol{a}}$ satisfying certain properties. The physics that we want to express in it is that the chain whose states are described by $\boldsymbol{c}(s)$ is confined to a tube formed by surrounding chains, and also surrounding plates. Inside the tube, the chain moves predominantly along its backbone. This motion, also called a reptation motion, can be seen as a diffusion along the backbone. The force generating diffusion in $\mathbf{R}^3$ is a gradient with respect to the position coordinate $\boldsymbol{r} \in \mathbf{R}^3$. The force generating diffusion along the backbone is thus a gradient with respect to s. In addition to the thermodynamic force $\Phi_{\boldsymbol{c}}$, we thus introduce a new force $(\Phi_{\boldsymbol{c}})_s$ (denoting the derivative of $\Phi_{\boldsymbol{c}}$ with respect to s).

The thermodynamic force generating dissipation in the motion of the plates has to be chosen in such a way that the constraint $tr\boldsymbol{a} = 1$ remains unchanged during the time evolution (Edwards et al. 2003). We can easily verify that the force

$$A_{ij} = \Phi_{a_{ij}} - \frac{1}{3} tr\Phi_a\, \delta_{ij} \tag{6}$$

has this property. Indeed, $d\boldsymbol{a}/dt = -\partial\Xi/\partial\Phi_a$ implies $dtr\boldsymbol{a}/dt = -tr\,(\partial\Xi/\partial\Phi_a) = 0$, provided the dissipation potential Ξ is a function of Å (i.e., it depends on $\Phi_{\boldsymbol{a}}$ only through its dependence on Å).

If we limit ourselves to states that are not too far from equilibrium (i.e., the states for which Φ_c and Φ_a are not too large), we can choose the dissipation potential Ξ to be the following quadratic function of the thermodynamic forces:

$$\Xi = \left(\Phi_{c_{ij}}\ ,\ \left(\Phi_{c_{ij}}\right)_s\ ,\ A_{ij}\right)\boldsymbol{\Lambda}\begin{pmatrix}\Phi_{c_{kl}}\\ \left(\Phi_{c_{kl}}\right)_s\\ A_{kl}\end{pmatrix}, \tag{7}$$

where

$$\boldsymbol{\Lambda} = \begin{pmatrix} \frac{\Lambda^{11}}{1-\alpha} & 0 & \frac{\Lambda^{13}}{\alpha(1-\alpha)} \\ 0 & \frac{\Lambda^{22}}{1-\alpha} & \frac{\Lambda^{23}}{\alpha(1-\alpha)} \\ \frac{\Lambda^{13}}{\alpha(1-\alpha)} & \frac{\Lambda^{23}}{\alpha(1-\alpha)} & \frac{\Lambda^{33}}{\alpha} \end{pmatrix} \tag{8}$$

Λ^{11}, Λ^{22}, Λ^{33}, Λ^{13}, and Λ^{23}, hereafter called mobility tensors, are phenomenological parameters representing the suspension in the model. By α, we denote the volume fraction of the suspended lamellae. In order for Eq. 7 to satisfy the properties required from the dissipation potential (see Appendix), the matrix $\boldsymbol{\Lambda}$ has to be positive definite. This then serves as a constraint for the phenomenological parameters Λ^{11}, Λ^{22}, Λ^{33}, Λ^{13}, and Λ^{23}.

In the absence of the lamellae (i.e., in the absence of the thermodynamic force Å), the dissipation potential Eq. 7 reduces to Ξ introduced in Eslami and Grmela (2008). The thermodynamic force $(\Phi_{\boldsymbol{c}})_s$ generates the reptation motion of the polymer chains. Now, we introduce the lamellae into the polymer melt. In the mathematical formulation, we express it by coupling the reptation force $(\Phi_{\boldsymbol{c}})_s$ to Å (i.e., $\Lambda_{23} \neq 0$). From the physical point of view, the coupling represents a modification of the diffusion along the backbone of the chain (i.e., the reptation motion) by the presence of the lamellae. The microscopic details of the lamellae–chain interactions are outside the scope of the mesoscopic formulation adopted in this paper. The newly introduced parameter Λ_{23}, quantifying the influence of the lamellae on the reptation, is considered as a phenomenological material parameter whose value is obtained by fitting experimental data.

As for the choice of the mobility tensors $\boldsymbol{\Lambda}$, we follow Beris and Edwards (1990, 1994) and use polynomial functions of $\boldsymbol{c}$ and $\boldsymbol{a}$. More specifically, we choose:

$$\boldsymbol{\Lambda}^{11} = \Lambda_0^{11}\left[f_1\widehat{\boldsymbol{c}\boldsymbol{\delta}} + f_2\widehat{\boldsymbol{c}\boldsymbol{c}}\right] \tag{9}$$

and

$$\boldsymbol{\Lambda}^{22} = \Lambda_0^{22}\left(1 + \widetilde{\Lambda_0^{22}}\left(tr\boldsymbol{c} - tr\boldsymbol{c}_{eq}\right)^2\right)\left[f_1\widehat{\boldsymbol{c}\boldsymbol{\delta}} + f_2\widehat{\boldsymbol{c}\boldsymbol{c}}\right] \tag{10}$$

$$\boldsymbol{\Lambda}^{33} = \Lambda_0^{33}\left(f_3\widehat{\boldsymbol{a}\boldsymbol{\delta}} + f_4\widehat{\boldsymbol{a}\boldsymbol{a}} + f_5\widehat{\boldsymbol{a}\boldsymbol{a}\boldsymbol{a}}\right) \tag{11}$$

$$\boldsymbol{\Lambda}^{13} = \Lambda_0^{13}\widehat{\boldsymbol{c}\boldsymbol{a}}$$

$$\boldsymbol{\Lambda}^{23} = \Lambda_0^{23}\widehat{\boldsymbol{c}\boldsymbol{a}} \tag{12}$$

The coefficients $f_i (i = 1 - 5)$ appearing in Eqs. 9, 10, and 11 equal either 0 or 1. We are introducing them in order to be able to explore in the next sections consequences of choosing linear and/or quadratic dependence on $\boldsymbol{c}$ and higher-order dependency of $\boldsymbol{a}$. If $(f_3 = 1,\ f_4 = 0,\ f_5 = 0)$ [respectively, $(f_4 = 1,\ f_3 = 0,\ f_5 = 0)$ or $(f_5 = 1,\ f_3 = 0,\ f_4 = 0)$], we call $\boldsymbol{\Lambda}^{33}$ a first-order (respectively, the second or third order) mobility tensor. The symbol $\boldsymbol{c}_{eq}$ arising in Eqs. 9 and 10 denotes the conformation tensor $\boldsymbol{c}$ at equilibrium. $\boldsymbol{\Lambda}$ are all fourth-order tensors; $\widehat{\ }$ means symmetrization in the four indices, and Λ_0^{11}, Λ_0^{22}, $\widetilde{\Lambda_0^{22}}$, Λ_0^{33}, Λ_0^{13}, and Λ_0^{23} are phenomenological coefficients.

The physical interpretation of the coefficients Λ_0 is the following: $(\Lambda_0)^{-1} \sim \lambda_0$ where λ_0 are relaxation times. In the two component fluids under consideration (polymers and lamellae), we need a mixing rule for the relaxation times. We choose the simplest one. We pass from λ_0^{11} to $(1-\alpha)\lambda_0^{11}$, from λ_0^{33} to $\alpha\lambda_0^{33}$, and from λ_0^{13} and λ_0^{23} to $\alpha(1-\alpha)\lambda_0^{13}$ and $\alpha(1-\alpha)\lambda_0^{23}$. The volume fraction α of the lamellae is related to the weight fraction w by $\alpha = \rho_c w/(\rho_a - (\rho_a - \rho_c)w)$, where ρ_c (respectively, ρ_a) is a mass density of the polymer (respectively, lamellae). The other place where the volume fraction α enters the governing Eqs. 3 and 4 is in the free energy discussed below.

Free energy

Finally, we turn to the specification of the free energy Φ. We write it as a sum of four terms:

$$\Phi = \Phi^{\text{kin}} + \Phi^c + \Phi^a + \Phi^{ca} \tag{13}$$

where $\Phi^{\text{kin}} = \frac{\boldsymbol{u}^2}{2\rho}$ is the kinetic energy part, ρ is the mass density assumed to be a constant, and Φ^c and Φ^a are the free energy of the polymer matrix, and the lamellae, respectively. The term Φ^{ca} is the contribution to the free energy due to the polymer–plate interaction.

As for the free energy of polymer matrix Φ^c, we follow what we have done in Eslami and Grmela (2008) by considering locally a FENE-P dumbbell model:

$$\Phi^c = \frac{1}{V}\int d\boldsymbol{r}\int_{-1}^{1} ds\Big[- n_c H Q_0^2 \ln\left(1 - tr\ \mathbf{c}\right) + Ktr(\boldsymbol{c}_s \cdot \boldsymbol{c}_s) - \frac{1}{2} n_c k_B T \ln(\det \mathbf{c})\Big] \tag{14}$$

By $\boldsymbol{c}_s$, we denote $\frac{d\boldsymbol{c}}{ds}$.

The first term is the FENE-P intramolecular energy, H is the modulus of the local spring, and R_0 its maximal length.

The second term represents a nonlocal (in s) contribution to the intramolecular energy. In the case when the local FENE-P dumbbell is replaced by a rigid dumbbell, it is the energy associated with the bending of the chain. The coefficient K is the modulus of this type of intramolecular interaction.

The third term represents the entropy S multiplied by the temperature T. By n_c, we denote the number density of the polymer chains ($n_c = \frac{(1-\alpha)\rho_c N_A}{M_c}$; α is the volume fraction of the lamellae, N_A is the Avogadro number, and M_c is the molecular weight of the polymer).

As for free energy of lamellae Φ^a, its energy part will be neglected. The entropy part is chosen to be a linear combination of the classical Boltzmann entropy and the Khokhlov–Semenov entropy (Khokhlov and Semenov 1985; Grmela 1990) accounting for the flexibility of the plates:

$$\Phi^a = G\ tr\boldsymbol{a} - \frac{1}{2} n_a \left(1 - K_{\text{flex}}\right) k_B T \ln(\det \mathbf{a}) + n_a K_{\text{flex}} k_B T tr\mathbf{a}^{-1} + \kappa n_a^2 k_B T \left((tr\boldsymbol{a})^2 - tr(\boldsymbol{a}\ .\ \boldsymbol{a})\right) \tag{15}$$

where n_a is the number density of plates ($n_a = \frac{\alpha}{A_0 h}$; A_0 is the surface area of the lamella and h is its thickness), K_{flex} denotes a parameter characterizing the flexibility of plates ($0 < K_{\text{flex}} < 1$), and κ is a modulus of the plate–plate interaction. The first term in the free energy expresses the constraint $tr\boldsymbol{a} = 1$, and the parameter G is the Lagrange coefficient.

Finally, the polymer lamellae interaction free energy Φ^{ca}, is chosen as follows:

$$\Phi^{ca} = \kappa'\ n_c n_a k_B T tr(\boldsymbol{c}\ .\ \boldsymbol{a}) \tag{16}$$

where κ' is phenomenological parameter measuring the polymer–plate topological interactions. The expression in Eq. 16 is the Onsager entropy adapted to the plate–chain topological interactions expressed in terms of the conformation tensors rather than distribution functions (see more in Eslami et al. 2007).

The choice of the parameters entering the free energy is restricted by requiring the thermodynamic stability, i.e., by requiring that the matrix

$$\begin{pmatrix} \Phi^c_{cc} & \Phi^{ca}_{ca} \\ \Phi^{ca}_{ca} & \Phi^a_{aa} \end{pmatrix}$$

is positive definite. We use the notation: $\Phi^c_{cc} = \frac{\partial^2 \Phi^c}{\partial c^2}$, $\Phi^a_{aa} = \frac{\partial^2 \Phi^a}{\partial a^2}$, and $\Phi^{ca}_{ca} = \frac{\partial^2 \Phi^{ca}}{\partial c \partial a}$.

When we are combining the free energies Φ^a, Φ^c, and Φ^{ca}, we have to face the problem of the disparity of shapes and sizes of the polymer macromolecules and the lamellae. Due to the large surface area of the rigid lamellae, one lamella interacts simultaneously with not one but a whole group of macromolecules. In other words, the particular shape and the rigidity of the lamellae makes its interaction with surrounding macromolecules (that are flexible and have a very different shape) very nonlocal. To account for this effect, we rescale n_a. We multiply it by a factor χ. After the rescaling, we can regard the lamellae and the macromolecules as equal partners in the interactions. In Eslami et al. (2007), the scaling parameter χ was assumed to be a constant. In this paper, we let it depend appropriately on the volume fraction α. The other parameters entering the free energy will, in general, also depend on α. However, we expect this dependence to be of lesser importance and leave it out of our consideration in this paper.

Material parameters

At this point we have completed the formulation of the governing equations of the model. In the next sections, we turn to their solutions. Before engaging ourselves in the process of finding solutions, we make a general comment about the parameters introduced in them. Every theory, formulated on any level of description, needs parameters (called material parameters) expressing the individual features of the systems under consideration. For instance, in classical mechanics, it is the mass and all the parameters entering the characterization of the forces; in hydrodynamics of simple fluids, the material parameters are the viscosity and the heat conductivity coefficients and all the parameters entering the local fundamental thermodynamic relation. The mapping physical systems $\rightarrow$ material parameters can be obtained by following two routes: (route 1) by staying inside the level, or (route 2) by investigating

relations to other levels. Below, we shall make a few brief comments about both routes.

Route 1

Let the level on which we place ourselves be denoted by the symbol $\mathcal{L}_0$. Among all experimental observations made on the level $\mathcal{L}_0$ (we shall denote them by the symbol $\mathcal{O}_0$), we select some ($\mathcal{O}_0^{\text{metr}} \subset \mathcal{O}_0$) that will be regarded as measurements of the material parameters. The values of the parameters are obtained by fitting the results of the observations $\mathcal{O}_0^{\text{metr}}$ with predictions of the theory. The success or the failure of the theory is then seen in comparison with the results of the remaining $\mathcal{O}_0 \setminus \mathcal{O}_0^{\text{metr}}$ observations with predictions of the theory. This route is traditionally followed on all well established levels as, for example, in classical thermodynamics, classical mechanics, and classical hydrodynamics.

Route 2

Let the level $\mathcal{L}_1$ be more microscopic (i.e., involving more details) than the level $\mathcal{L}_0$. For instance, let $\mathcal{L}_0$ be the level of classical hydrodynamics and $\mathcal{L}_1$ the level of Boltzmann kinetic theory. Both levels $\mathcal{L}_0$ and $\mathcal{L}_1$ are autonomous (i.e., neither of them needs the other to be formulated and applied), but since the level $\mathcal{L}_1$ is more microscopic, we can anticipate that an analysis of solutions of the governing equations on the level $\mathcal{L}_1$ can lead to a derivation of the theory on the level $\mathcal{L}_0$. The process of the derivation can be seen as a pattern recognition process in the set of solutions (trajectories) obtained on the level $\mathcal{L}_1$. For instance, in the case of $\mathcal{L}_1$ being the Boltzmann kinetic theory and $\mathcal{L}_0$ the hydrodynamics, such passage $\mathcal{L}_1 \to \mathcal{L}_0$ is provided by the famous Chapman–Enskog method. Let the material parameters associated with the level $\mathcal{L}_1$, respectively, $\mathcal{L}_0$, be denoted $\mathcal{P}_1$, respectively, $\mathcal{P}_0$. The passage $\mathcal{L}_1 \to \mathcal{L}_0$ induces the passage $\mathcal{P}_1 \to \mathcal{P}_0$. The material parameters $\mathcal{P}_0$ can be thus obtained by independent measurements made on the level $\mathcal{L}_1$. For example, by using the Chapman–Enskog method, we obtain the viscosity and the heat conductivity coefficients expressed in terms of the material parameters used in the Boltzmann kinetic theory.

In the context of the model introduced in this paper, we note first that the material parameters all have a clear physical meaning. Each of them appears in either the free energy or the dissipation potential; each of them is associated with specific physics expressed on the mesoscopic level on which the model is formulated. We do not attempt in this paper to see the suspensions under consideration from a more microscopic point of view (e.g., from the point of view of kinetic theory), and consequently, our only option to specify the material parameters is route 1. The main problem is that we do not have in our disposition a large enough pool of experimental data to both measure and predict. The post processing of the model, i.e., a systematic analysis of the influence of the material parameters on the results that are compared with results of experimental observations, that we do in the next section, is found to be very useful in the determination of the mapping physical systems $\to$ material parameters.

Results and discussion

As for the imposed flows, we consider shear flows and oscillatory flows. We calculate both the linear and the nonlinear viscoelastic behavior.

A simple shear flow is given by the momentum field $u_1 = \dot{\gamma}_{(t)} x_2$, $u_2 = u_3 = 0$. The velocity gradient $\dot{\gamma}_{(t)}$ is, in general, a function of time. The absolute value of $\dot{\gamma}_{(t)}$ is called a shear rate. In this paper, we follow the standard notation for the viscosity coefficient η, the shear stress σ, and the first normal stress differences N_1. The governing equations of the model represent, from the mathematical point of view, a system of partial differential equations (PDEs). The initial conditions are the equilibrium solutions (i.e., $\Phi_c = 0$ and $\Phi_a = 0$). As for the boundary conditions of PDEs, we follow Eslami and Grmela (2008). We solve the time evolution equations numerically by using the MATHEMATICA software package (Wolfram 1991).

In the linear viscoelastic regime with small sinusoidal strain $\gamma(t) = \gamma_0 \sin \omega t$, the shear stress tensor is presented by $\sigma(t) = \gamma_0 \left(G' \sin \omega t + G'' \cos \omega t\right)$, where G' and G'' are the storage and loss moduli, respectively. Again, in order to model the linear viscoelastic behavior of nanocomposites, we shall follow the procedure used in Eslami and Grmela (2008) and express the conformation tensors $\boldsymbol{c}$ and $\boldsymbol{a}$ as a linear function of $\gamma_0 \omega$. Finally, we solve the reduced equations numerically to find the linear viscoelastic functions.

Model predictions

We turn now to the postprocessing of the model, i.e., to finding the relation between model parameters and rheological measurements in different flows.

It is useful to regard rheological models as input–output systems. The input is the microscopic or mesoscopic physics used in its formulation and the output are predictions of the observed rheological behavior. Both input and output have many components. In the

input, they are the particular physical features involved (e.g., the local extensibility, the constraints, tube formation, etc.), and in the output, they are the features of the observed behavior (e.g., the length of the plateau in the curve η vs $\dot{\gamma}$ for pure polymer, the slope of this curve as $\dot{\gamma} \to \infty$, the slope of this curve at low shear rate which is an indication of yield stress, etc.). The passage between the input and the output is made by solving the (in general, very nonlinear) governing equations of the model. An understanding gained by the model is often measured by the success in establishing direct passages between individual components of the input and individual components of the output. For example, as we shall see below, the nonlinear dependence of the dissipative kinetic coefficients is seen to influence mainly the length of the plateau in the case of pure polymer, the nonlocal intramolecular interactions influence mainly the linear rheological behavior, dependency of rescaling parameter to clay volume fraction influences the material function at low shear rate and low frequency, etc. A word of caution is in order. The input–output passage involves solutions of complex nonlinear equations. In general, the input–output relation is very complex, and simple passages between single components of the input and the output do not exist. Having this in mind, we proceed to investigate the input–output passage of the model presented in this paper.

In the following calculations of model predictions, the model parameters are chosen as follows: $\Lambda_0^{11} = 10^{-5}$, $\Lambda_0^{22} = 10^{-7}$, $\widetilde{\Lambda_0^{22}} = 1.75 \times 10^5$, $\Lambda_0^{33} = 10^{-8}$, $\Lambda_0^{23} = 10^{-8}$, $\Lambda_0^{13} = 10^{-8}$, $b = \frac{2HQ_0^2}{k_B T} = 2.5$, $K = 3 \times 10^5$, $\kappa = 10^{-24}$, $\kappa' = 10^{-24}$, $K_{\text{flex}} = 0.1$, $\chi = 6000\,\alpha^{0.75}$ and $\xi = 0.99$. Prediction of transient material functions is made at $\dot{\gamma} = 0.1 s^{-1}$ and 5 wt.% clay.

Effects of the shear rate on transient material functions

Figure 1a, b depicts the effects of shear rate on the transient material functions, η^+ and N_1^+, respectively. The results show that, for small shear rates, the viscosity reaches its steady state value monotonically.

As the shear rate increases, the curve of viscosity vs time shows an overshoot. The size of the overshoot increases and the time at which the overshoot appears decreases when the shear rate increases. Similar results are obtained for the first normal stress differences (see Fig. 1b). The overall qualitative features of the curves are essentially the same as the ones seen in the experimental data collected for polymer melts and solutions (Bird et al. 1987; Eslami et al. 2003), miscible polymer blend (Eslami et al. 2004), and polymer nanocomposites (Wu et al. 2005; Ayyer and Leonov 2004).

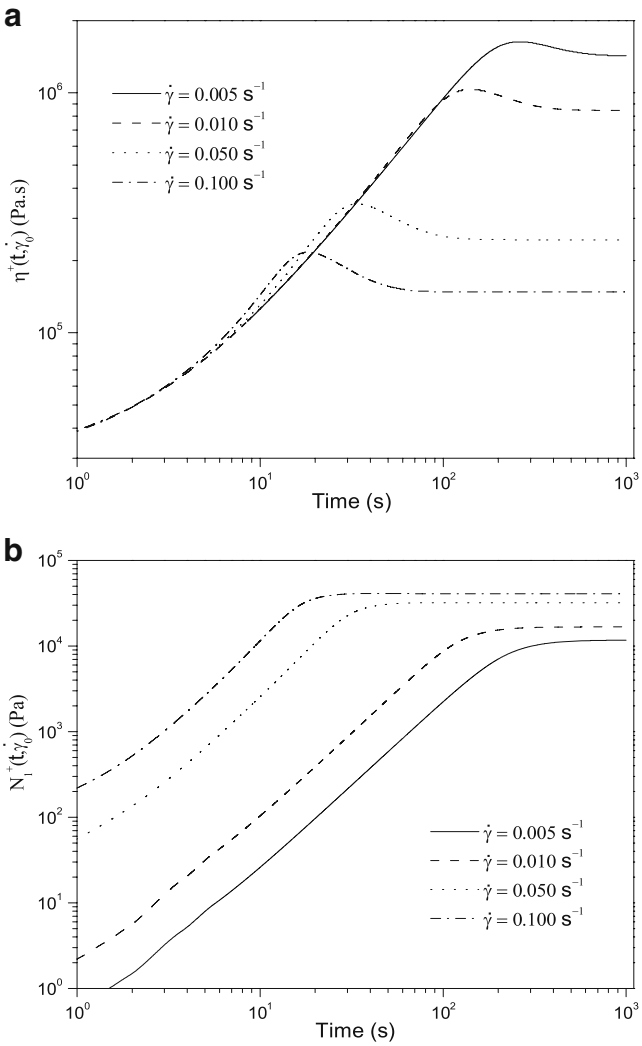

Fig. 1 Effect of shear rate on stress growth material functions. **a** Shear stress and **b** first normal stress differences

Effects of the mobility coefficients on the material functions

Figure 2a, b depicts the influence of the plate mobility coefficient Λ_0^{33} on the transient material functions, η^+ and N_1^+, respectively. As seen in Fig. 2a, both the stationary value and the size of the overshoot increase with decreasing Λ_0^{33}. Figure 2b indicates that similarly as the shear viscosity, the stationary values of the first normal stress difference increase with decreasing Λ_0^{33}. However, N_1^+ is less sensitive to increasing the size of the overshoot than η^+ (the size of the overshoots becomes visible more clearly if the curves are drawn in the normalized form).

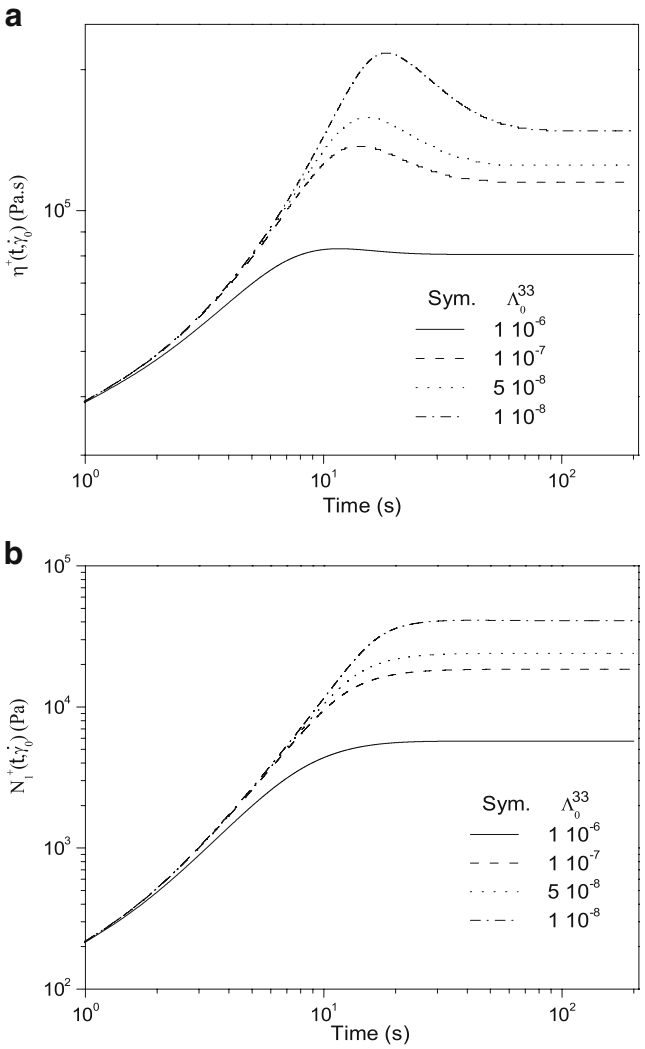

Fig. 2 Effect of plate mobility coefficient Λ_0^{33} on stress growth material functions. **a** Shear viscosity and **b** first normal stress differences

Changing the plate mobility coefficient means, from the physical point of view, changing the friction among the plates. With the plate mobility coefficient increasing, the friction among the platelets decreases, which in turn means a decrease in the obstacles in the suspension and, thus, a decrease in the viscosity.

As for the overshoot in the viscosity curve, we can interpret it as follows: With decreasing plate mobility coefficient, the friction among platelets increases which then means that the suspension is more anisotropic and consequently the overshoots are more pronounced. It should be also noted that we let the plate mobility depend on the plate orientation tensor $\boldsymbol{a}$ (see Eq. 11). From the physical point of view, the higher the order on the nonlinearity of the function $\Lambda(\boldsymbol{a})$ is, the more anisotropic the suspension is.

Figure 3a, b presents the influence of the polymer plate mobility coefficients Λ_0^{13} and Λ_0^{23} on the stress growth viscosity. The former is related to the classical dissipation mechanism and the latter to the reptation mechanism.

Again, one can relate the interaction mobility coefficient to the friction among the macromolecules and plates: Λ_0^{13} is related to the friction among polymer chains and platelets, while Λ_0^{23} can be interpreted as the level of friction between the chain segments and the platelets.

Figure 3a shows that, with increasing Λ_0^{13}, the stationary values of the shear viscosity increase. One can also see slight changes in the size of the overshoot with increasing Λ_0^{13}. As mentioned above, increasing Λ_0^{13} means increasing the interaction between chains and

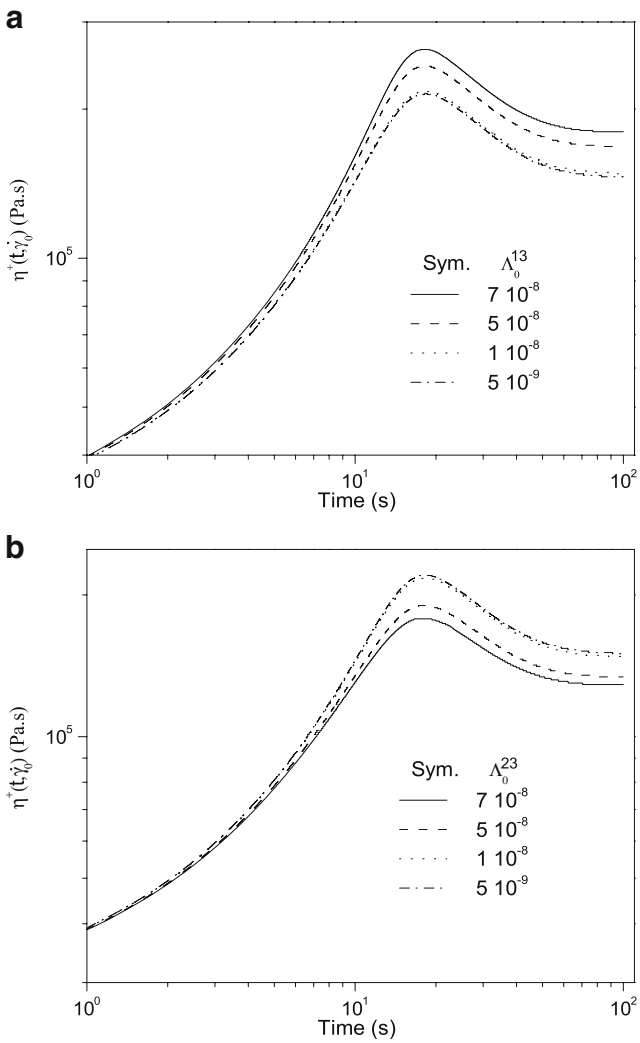

Fig. 3 Effect of polymer plate interaction mobility coefficient on stress growth viscosity. **a** Effect of Λ_0^{13} and **b** effect of Λ_0^{23}

platelets. Depending on the morphology of the chain, this interaction manifests itself differently. At low shear rates the coil-like morphology of the chains offers more obstacles for the motion of the platelets, and, consequently, we see the viscosity increase (i.e., the friction among polymer chains and platelets increases). However, at high shear rates, where the chains are more extended and oriented, increasing the interaction mobility coefficient of polymer and plate means decreasing the friction among polymer chain and platelets, which then decreases the viscosity of the suspension (results for high shear rates are not shown here for the sake of brevity).

Figure 3b shows that, with increasing Λ_0^{23}, the stationary value of the shear viscosity decreases while the size of the overshoot does not change. The same interpretation as above can also explain this behavior. As mentioned earlier, Λ_0^{23} is related to the interaction between chain segments and platelets, and since we assume that the segments are very small (for more detail, see Eslami and Grmela 2008), the flow situation (low or high shear rates) does not change the overall behavior of this curve.

Effects of the nanoparticle loading on the material functions

As mentioned earlier, the volume fraction of nanoparticle α is introduced in three places: in the dissipation potential, in the free energy, and in the rescaling parameter. The reason why we let the rescaling parameter be a function of the volume fraction of the silicate plates is that the number of polymer macromolecules that are in contact with a plate changes when the number of plates changes. At this point, we assume a simple dependency of the rescaling parameter to α.

The transient shear stress and the first normal stress differences of polymer nanocomposites at different contents of nanoparticles are presented in Fig. 4a, b. As expected, the rheology of polymer nanocomposites is significantly influenced by the nanoparticle loading. As it increases, i.e., as α increases, the effects become more significant. These results show that both the stationary values and the size of the overshoots increase with increasing the nanoparticle loading. The dependence of the overshoots on α is more pronounced in σ^+ than in N_1^+. The stationary values of N_1^+ (i.e., $N_1^+|_{t\to\infty}$) depend on α more sensitively than the stationary values of the shear stress. From the physical point of view, this is because, by increasing the clay loading, the elasticity increases, which then shows itself in the overshoot in the shear stress and in the absolute values of the first normal stress differences.

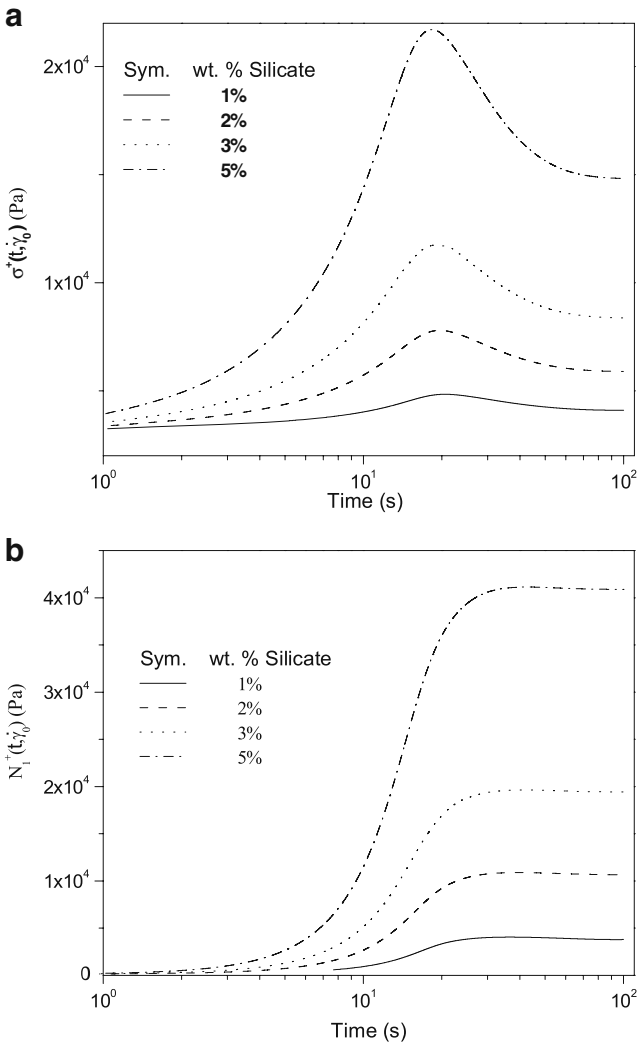

Fig. 4 Effect of the nanoparticle weight fraction on stress growth material functions. **a** Shear stress and **b** first normal stress differences

Figure 5a shows the steady state viscosity of polymer nanocomposites for a wide range of shear rates and different nanoparticle contents. It is found that increasing the clay loading results in a significant increase in the viscosity at low shear rates and, to a lesser extent, at high shear rates. In other words, when the nanoparticle loading increases, the behavior for all ranges of shear rates becomes non-Newtonian (shear thinning). The model prediction shows that, at high shear rates, the viscosity is almost independent of the silicate loading and is comparable to that of the polymer matrix. This is because, at high shear rates, the plates are all oriented in the direction of the flow and the viscosity of the suspension is dominated by the polymer matrix. The effect of the clay loading at low shear rates is depicted in the small figure imbedded in Fig. 5a. As it is clearly

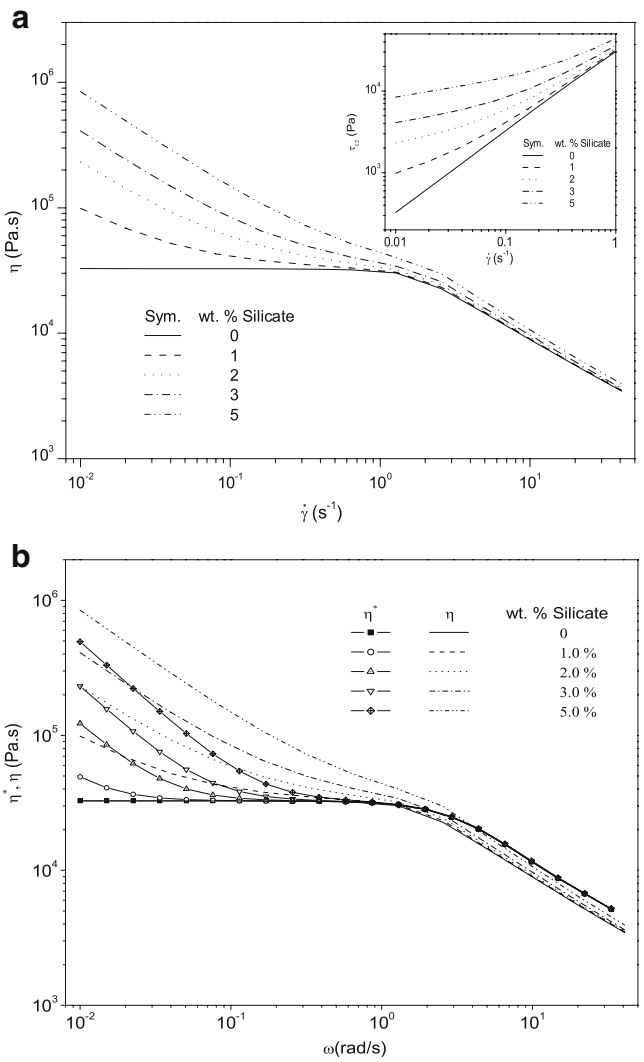

Fig. 5 Effect of the nanoparticle weight fraction on the **a** steady state viscosity and **b** Cox-Merz relation

seen in this figure, the slope of the curve of shear stress vs shear rate decreases with increasing clay loading, and at high clay loading, it almost becomes a plateau, which indicates a large value of the yield stress. We will discuss this issue in Fig. 8, where we compare the model with experimental data.

The empirical Cox–Merz relation, which requires $\eta^*(\omega) = \eta(\dot{\gamma})$ where $\omega = \dot{\gamma}$, is proved to be applicable for homopolymers. Figure 5b shows that the rule fails for polymer nanocomposites. Even though our model does not predict well the Cox–Merz relation for the polymer matrix at high shear rates, it does predict it for low and medium shear rates. In the case of nanocomposites the Cox–Merz rule fails in the whole range of shear rates. Such a failure has been previously observed for filled polymer systems. The reason for the failure is that, by applying steady shear flow, the silicate layers become preferentially oriented in the direction of the flow, even at low shear rates. The failure of the Cox–Merz rule can also be related to the formation of a network structure of silicate layers. An extension of the Cox–Merz rule concentrated suspensions and materials with a yield stress has been introduced by Doraiswamy et al. (1991). We hope to discuss this issue in near future.

Figure 6a, b represents the linear viscoelastic behavior as a function of the angular frequency for polymer nanocomposites at different nanoparticle loading. As we have already seen in Fig. 5a, the flow behavior of nanocomposites differs significantly from the one corresponding to the pure matrix fluid in the non-linear viscoelastic zone. Results of Fig. 6a show that

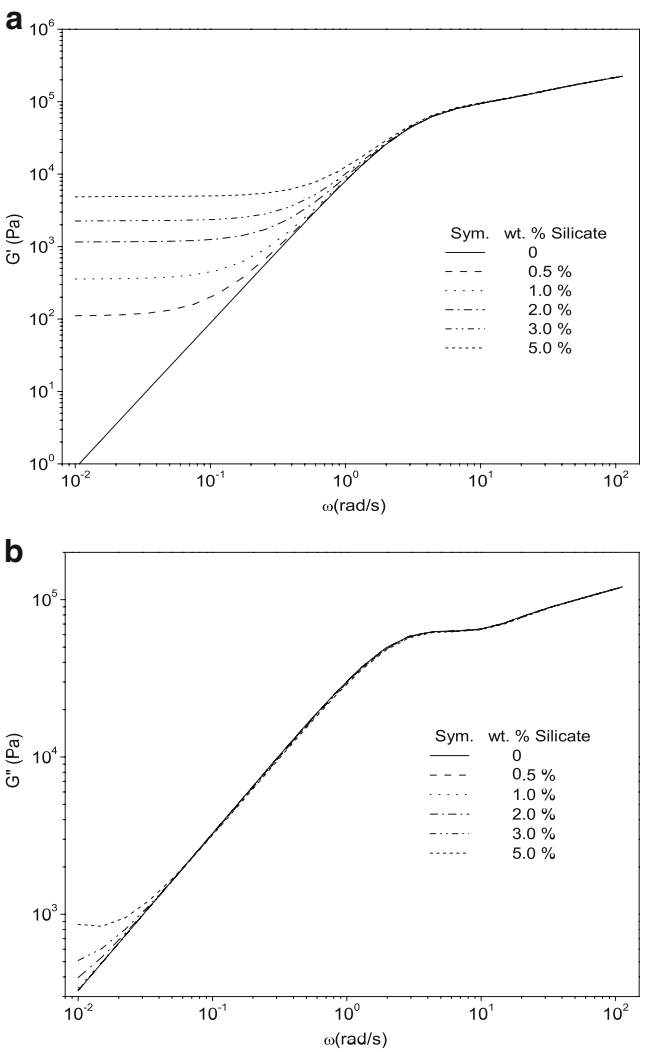

Fig. 6 Effect of the nanoparticle weight fraction on the **a** storage modulus G' and **b** loss modulus G''

the storage modulus G' is dramatically influenced by the presence of silicate platelets, while Fig. 6b shows a lesser sensitivity of loss modulus G'' on the clay loading. As seen from Fig. 6a, the slopes of $\log G'$ vs $\log \omega$ are much smaller than 2, which is normally expected to be the case for noncrosslinked polymer melts. Such large deviation, which normally occurs in the presence of a small amount of layered silicate loading, may be due to the formation of a clay network structure. In general, the model predictions are qualitatively consistent with experimental data for polymer layered silicate nanocomposites (Wu et al. 2005; Ayyer and Leonov 2004; Krishnamoorti et al. 2001; Ren and Krishnamoorti 2003).

Comparison with experimental data

Model predictions are compared with a complete set of experimental data for polymer/layerd silicate nanocomposites in steady and oscillatory shear flows. The experimental data has been taken from Krishnamoorti et al. (2001) and Ren and Krishnamoorti (2003) where the rheological tests were performed over a wide range of shear rate and angular frequency. In the comparison between model predictions and experimental data, the model parameters are considered to be: $\Lambda_0^{11} = 2 \times 10^{-7}$, $\Lambda_0^{22} = 3 \times 10^{-6}$, $\widetilde{\Lambda_0^{22}} = 1.5 \times 10^4$, $\Lambda_0^{33} = 8 \times 10^{-10}$, $\Lambda_0^{13} = 2 \times 10^{-10}$, $\Lambda_0^{23} = 5 \times 10^{-10}$, $b = 2.5$, $\kappa = 10^{-25}$, $\kappa' = 10^{-25}$, $K_{\text{flex}} = 0.15$, $\chi = 800\,\alpha^{0.75}$, $\xi = 0.98$, $K = 3 \times 10^5$.

Figure 7a, b shows the effect of clay loading on the steady state viscosity and first normal stress differences, respectively. As can be seen in Fig. 7a, this set of experimental data is very well predicted by the model over the whole range of extended shear rates. In order to faithfully compare model I and model II, we use the same experimental data that have been used in Eslami et al. (2007). We found that the prediction of model II is much closer to experimental data than model I, especially at high silicate loading.

The melt elasticity of polymeric systems can be measured by the first normal stress differences N_1. The effect of silicate loading on the elasticity of polymer nanocomposites has been previously investigated by measuring the dependence of N_1 on the clay loading (Gupta et al. 2005; Krishnamoorti et al. 2001; Ren and Krishnamoorti 2003). According to Gupta et al. (2005), in the case of exfoliated nanocomposites, the melt elasticity of nanocomposites decreases with an increase in clay loading. The authors claimed that this reduction of the elasticity may be related to the high interaction between clay layers and polymer chains in the case of exfoliated nanocomposites.

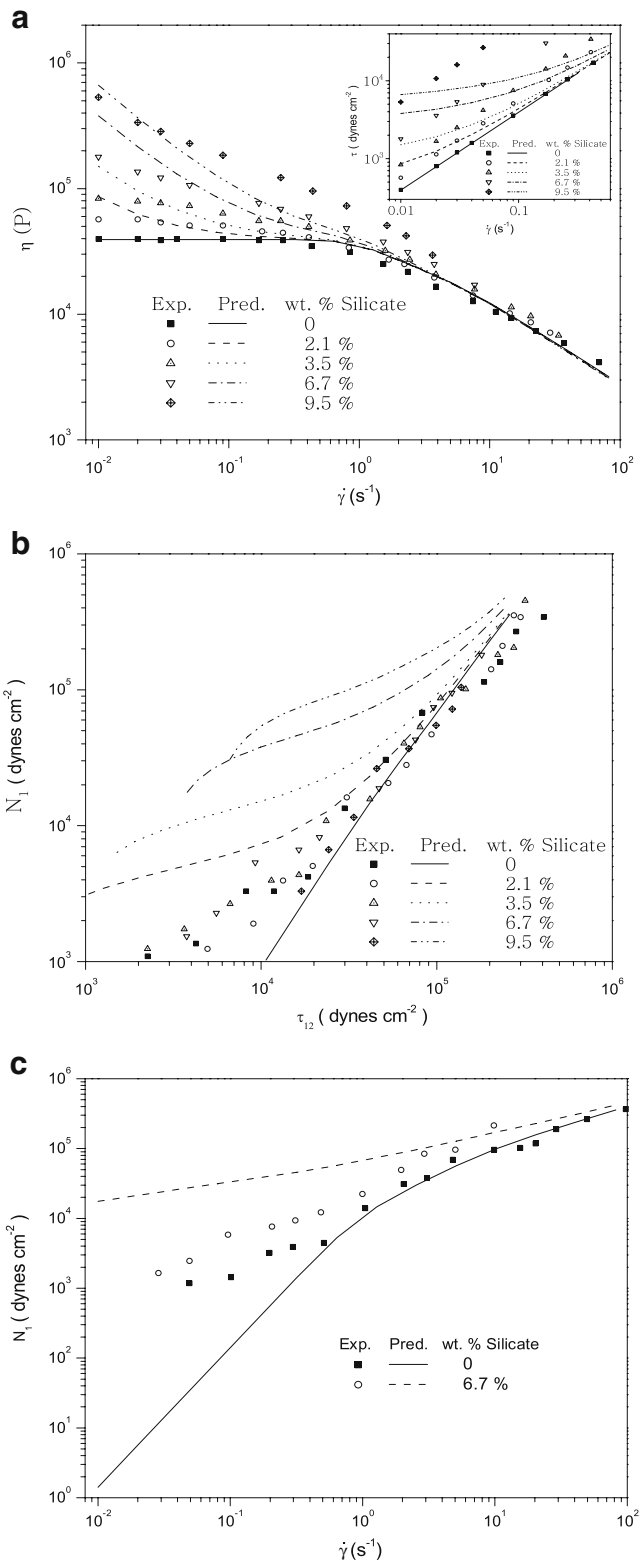

Fig. 7 Model predictions and comparison with experimental data in steady shear flow. **a** Steady viscosity, **b** steady first normal stress vs shear stress, and **c** steady first normal stress vs shear rate

Krishnamoorti et al. (2001) and Ren and Krishnamoorti (2003) also measured the first normal stress differences N_1 as a function of the shear stress at different clay loading. They reported that N_1 is independent of the silicate loading (see Fig. 7b). The authors suggest that this observation can be a consequence of the flow-induced orientation of silicate layers.

We also compared our model predictions with experimental data reported in Krishnamoorti et al. (2001) and Ren and Krishnamoorti (2003). As seen in Fig. 7b, our predictions do not agree with their observations. In other words, with an increase in clay loading, the first normal stress difference N_1 increases. We suggest that the increase of the value of N_1 is a consequence of the solid-like behavior of nanocomposites (becoming stronger with an increase in clay loading). Our results show that, at high shear stress (high shear rates), N_1 is nearly independent of the clay loading. This observation at high shear stress is in agreement with experimental observation in Krishnamoorti et al. (2001) and Ren and Krishnamoorti (2003). It should also be noted that an unusual decrease in N_1 is observed at very low shear rates.

In Fig. 7c, we plot N_1 vs shear rate, where the model predictions are compared with experimental data. Again, we see a less satisfactory agreement between the model predictions and the experimental data, especially at low shear rates.

One of the highlighted characteristics of the rheology of the filled polymer system, especially at high concentration, is the emergence of the yield stress. This means that, at stresses that are lower than yield stress, the suspension behaves like a solid (it deforms only elastically), while at stresses that are higher than the yield stress, it behaves like a liquid. From the physical point of view, the emergence of the yield stress is related to high filler–filler interactions, which become important at concentrated suspensions. According to Casson, the yield stress can be determined by the following equation (Malkin 1990):

$$\sigma_{12}^{1/2} = \sigma_0^{1/2} + \beta\, \dot{\gamma}^{1/2}, \tag{17}$$

where σ_0 is yield stress and β is an arbitrary constant.

Figure 8a shows the prediction of the model for the shear stress vs shear rate at low shear rates where we calculate the yield stress. The yield stress is calculated by fitting Eq. 17 for different clay loading (see the small graph imbedded in Fig. 8a).

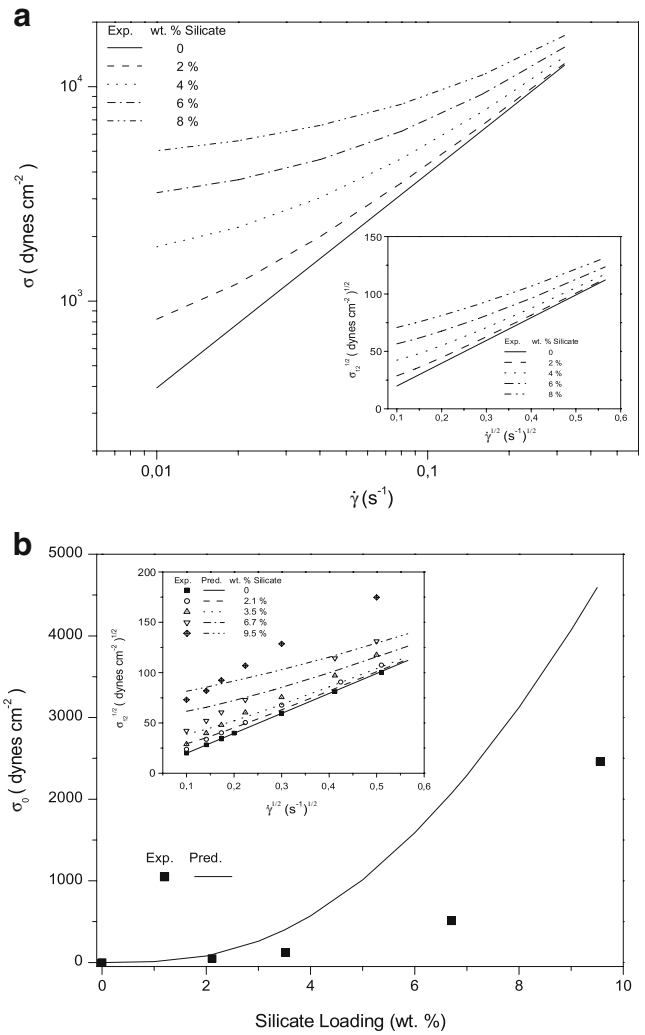

Fig. 8 Model predictions and comparison with experimental data. **a** Yield stress at different silicate loading, model predictions. **b** Yield stress, comparison between model and experimental data

Yield stresses predicted by the model are also compared with experimental data (see Fig. 8b). The results indicate that the model predictions overestimate the yield stress, especially at high silicate loadings. These results are qualitatively in agreement with highly shear thinning behavior of nanocomposites with high silicate loading at low shear rates (upward viscosity at low shear rates).

Model predictions are also compared with linear viscoelastic properties of polymer/layerd silicate nanocomposites obtained by Krishnamoorti et al. (2001) and Ren and Krishnamoorti (2003). The extension of the experimental angular frequency ω window was obtained using the time temperature superposition.

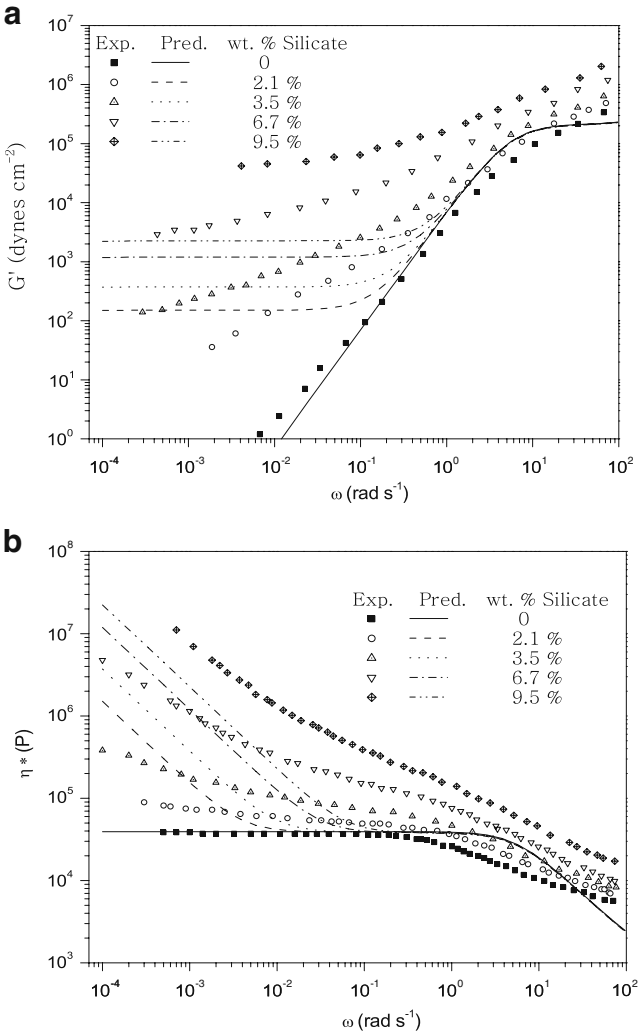

Fig. 9 Model predictions and comparison with experimental data in oscillatory shear flow. **a** Storage modulus G' and **b** complex viscosity η^*

The storage modulus G' and complex viscosity η^* are presented at the reference temperature $T_0 = 85°C$. Figure 9a, b shows the model predictions with this set of experimental data. As it is clear from these figures, the model is able to capture qualitatively the overall feature of polymer/layerd silicate nanocomposites, namely, plateau in G' at low frequency and upward complex viscosity at low frequency. However, the quantitative agreement is less satisfactory. In general, the reasons for the less satisfactory agreement may be partially due to the fact that the silicate lamellae in experimentally prepared suspensions are rarely completely exfoliated, and consequently, some new physical processes, that are not included in our model, become important.

Conclusion

A mesoscopic rheological model of a spatially homogeneous and isothermal suspension of completely exfoliated clay lamellae in polymer melts is formulated. Due to polymer–polymer and polymer–plate interaction, macromolecules of the polymer melt are effectively confined into tube formed by other macromolecules and the plates. The mesoscopic formulation does not allow us, however, to enter into microscopic details of the mechanism involved in the lamellae participation in the reptating motion. The model is constructed by combining the mesoscopic rheological model of polymer/layered silicate nanocomposites (Eslami et al. 2007) with the mesoscopic rheological model of melts composed of reptating macromolecules (Eslami and Grmela 2008). Having chosen the state variables, the model is formulated by, first, writing down a framework for the governing equations (guaranteeing the compatibility with mechanics and thermodynamics) and, second, filling the framework by specifying the kinematics of the state variables, the free energy, and the dissipation potential. The mesoscopic level of description chosen in this paper appears to be a good compromise between microscopic details and overall simplicity of the governing equations. On the one hand, we are able to express in the model important features of the physics involved (like, for example, reptation of polymer chain, polymer–plate and plate–plate interactions) and, on the other hand, the governing equations are easily solved numerically by standard software packages. The calculated rheological data for steady, transient, and oscillatory shear flows are reported. Particular attention is payed to the region of low shear rate and low frequency. The results show that the model is able to capture the overall rheological behavior of polymer-layered silicate nanocomposites.

An important issue that still remains to be considered in more detail is the case when the lamellae are not completely exfoliated. The challenge is to identify the physical processes that become important in this situation and to express them in the model. The framework of the model will remain unchanged since we shall again require the agreement of model predictions with the observed compatibility with thermodynamics.

Acknowledgements The authors acknowledge the financial support provided by the Natural Sciences and Engineering Research Council (NSERC) of Canada.

Appendix: GENERIC framework

Let x denote the state variables. If we limit ourselves to isothermal and incompressible fluids, then the compatible with thermodynamics and mechanics time evolution of x is governed by Grmela (1984, 1986, 1991, 2002), Beris and Edwards (1994), Grmela and Ottinger (1997), Ottinger and Grmela (1997), and Ottinger (2005)

$$\dot{x} = L\Phi_x - \frac{\partial \Xi}{\partial \Phi_x} \tag{18}$$

called in Grmela and Ottinger (1997) and Ottinger and Grmela (1997) GENERIC. By $\dot{x}$, we denote the time derivative of x. The first term on the right-hand side of Eq. 18 expresses the compatibility with mechanics, the second the compatibility with thermodynamics. The symbols appearing in Eq. 18 have the following meaning.

Free energy

$\Phi(x)$, a real valued function of x, has the physical meaning of the total free energy. By Φ_x, we denote the derivative of Φ with respect to x.

Kinematics

The operator L, hereafter called a Poisson bivector, transforms a covector (a gradient of a potential) into a vector. From the physical point of view, L expresses kinematics of the state variables x. In the particular case of classical mechanics of particles (the state variables in this case are $x = (p, q)$, where q are position vectors and p the momenta of the particles), $L = \begin{pmatrix} 0 & 1 \\ -1 & 0 \end{pmatrix}$. This is the Poisson bivector transforming in classical mechanics the gradient of energy $E(q, p)$ into a vector field. In the general setting, L is required to satisfy the following properties: $\{A, B\} =< A_x, LB_x >$ is a Poisson bracket, i.e., $\{A, B\} = -\{B, A\}$, and satisfies the Jacobi identity $\{A, \{B, C\}\} + \{B, \{C, A\}\} + \{C, \{A, B\}\} = 0$; A, B, C are sufficiently regular real valued functions of x; and $<, >$ denotes the inner product.

Dissipation

$\Xi(\Phi_x)$, called a dissipation potential, is a sufficiently regular real valued function of Φ_x satisfying the following properties: (1) $\Xi(0) = 0$, (2) Ξ reaches its minimum at 0, (3) Ξ is concave in a neighborhood of 0.

Properties of solutions of Eq. 18

The properties required from L, Ξ appearing in Eq. 18 imply that solutions to Eq. 18 satisfy the following inequality:

$$\frac{d\Phi}{dt} \leq 0 \tag{19}$$

The free energy Φ can thus only remain unchanged or decrease during the time evolution. To see that Eq. 19 indeed holds, we note that $\frac{d\Phi}{dt} =< \Phi_x, L\Phi_x > - < \Phi_x, \frac{\partial \Xi}{\partial \Phi_x} > \leq 0$. The last inequality follows from $< \Phi_x, L\Phi_x >= 0$ and from the properties required from the dissipation potential Ξ. The inequality Eq. 19 together with the thermodynamic stability requirement (i.e., Φ is a convex function of x) allows us to consider Φ as a Lyapunov function. This then means that solutions to Eq. 18 tend, as $t \to \infty$, to states that minimize the free energy (i.e., the states, called equilibrium states, that are solutions of $\Phi_x = 0$).

References

Ayyer RK, Leonov AI (2004) Comparative rheological studies of polyamide-6 and its low loaded nanocomposite based on layered silicates. Rheol Acta 43:283–292

Beris AN, Edwards BJ (1990) Poisson bracket formulation of viscoelastic flow equations of differential type: a unified approach. J Rheol 34:55–78

Beris AN, Edwards BJ (1994) Thermodynamics of flowing systems, 1st edn. Oxford University Press, New York

Bird RD, Armstrong RC, Hassager O (1987) Dynamic of polymeric fluids, vol 1. Wiley, New York

Bousmina M (2006) Study of intercalation and exfoliation processes in polymer nanocomposites. Macromolecules 39:4259–4263

De Gennes PG (1971) Reptation of a polymer chain in the presence of fixed obstacles. J Chem Phys 55:572–579

Doi M, Edwards SF (1986) The theory of polymer dynamics. Oxford University Press, New York

Doraiswamy D, Mujumdar AN, Tsao I, Beris AN, SDanforth C, Metzner AB (1991) The CoxMerz rule extended: a rheological model for concentrated suspensions and other materials with a yield stress. J Rheol 35:647–685

Edwards BJ, Dressler M, Grmela M, Ait-Kadi A (2003) Rheological models with microstructural constraints. Rheol Acta 42:64–72

Eslami H, Grmela M (2008) Mesoscopic formulation of reptation. Rheol Acta 47:399–415

Eslami H, Ramazani A, Khonakdar HA (2003) Volume preserving conformational rheological models for multi-component miscible polymer blends using the GENERIC formalism. Macromol Theory Simul 12:524–530

Eslami H, Ramazani A, Khonakdar HA (2004) Predictions of some internal microstructural models for polymer melts and solutions in shear and elongational flows. Macromol Theory Simul 13:655–664

Eslami H, Grmela M, Bousmina M (2007) A mesoscopic rheological model of polymer/layered silicate nanocomposites. J Rheol 51:1189–1222

Grmela M (1984) Particle and bracket formulations of kinetic equations. Contemp Math 28:125–132

Grmela M (1985) Stress tensor in generalized hydrodynamics. Phys Lett A 111:41–44

Grmela M (1986) Bracket formulation of diffusion-convection equations. Physica D 21:177–212

Grmela M (1990) Thermodynamic and rheological modeling: polymeric liquid crystals. In: Collyer AA, Utracki LA (eds) Polymer rheology and processing. Elsevier, Amsterdam, pp 55–81

Grmela M (1991) Mesoscopic dynamic and thermodynamic: application to polymer fluids. Lect Notes Phys 381:99–126

Grmela M (2002) Reciprocity relations in thermodynamics. Physica A 309:304–328

Grmela M, Ottinger HC (1997) Dynamics and thermodynamics of complex fluids. I. Development of a general formalism. Phys Rev E 55:6620–6632

Gu JF, Grmela M (2008) GENERIC model of active advection. J Non-Newton Fluid Mech 13:12–26

Gupta RK, Pasanovic-Zujo V, Bhattacharya SN (2005) Shear and extensional rheology of EVA/layered silicate-nanocomposites. J Non-Newton Fluid Mech 128:116–125

Khokhlov AR Semenov AN (1985) On the theory of liquid-crystalline ordering of polymer chains with limited flexibility. J Stat Phys 38:161–182

Krishnamoorti R, Ren J, Silva AS (2001) Shear response of layered silicate nanocomposites. J Chem Phys 114:4968–4972

Likhtman AE, McLeish TCB (2002) Quantitative theory for linear dynamics of linear entangled polymers. Macromolecules 35:6332–6343

Malkin AY (1990) Rheology of filled polymer. Adv Polym Sci 96:69–97

McLeish TCB (2002) Tube theory of entangled polymer dynamics. Adv Phys 51:1379–1527

Ottinger HC (2005) Beyond equilibrium thermodynamics. Wiley, New York

Ottinger HC, Grmela M (1997) Dynamics and thermodynamics of complex fluids. II. Illustrations of a general formalism. Phys Rev E 56:6633–6655

Ren J, Krishnamoorti R (2003) Nonlinear viscoelastic properties of layered silicate based intercalated nanocomposites. Macromolecules 36:4443–4451

Wolfram S (1991) Mathematica-A system for doing mathematics by computer, 2nd edn. Wesley-VCH, New York

Wu D, Zhou Ch, Hong Z, Mao D, Bian Z (2005) Study on rheological behaviour of poly(butylene terephthalate)/montmorillonite nanocomposites. Eur Polym J 41:2199–2207